Design of Thermochromic Luminescent Dyes Based on the Bis(*o*-carborane)-Substituted Benzobithiophene Structure

Kenta Nishino[1], Yasuhiro Morisaki[1,2], Kazuo Tanaka[1]* and Yoshiki Chujo[1]

[1]*Department of Polymer Chemistry, Graduate School of Engineering, Kyoto University, Katsura, Nishikyo-ku, Kyoto 615-8510, Japan*

[2]*Present address: Department of Applied Chemistry for Environment, School of Science and Technology, Kwansei Gakuin University, 2-1 Gakuen, Sanda, Hyogo 669-1337, Japan*

E-mail: tanaka@poly.synchem.kyoto-u.ac.jp

Abstract

To obtain solid-state emissive materials having stimuli-responsive luminescent chromic properties without phase transition, benzobithiophenes modified with two *o*-carborane units having various substituents in the adjacent phenyl ring in *o*-carborane were designed and synthesized. Their emission colors were strongly affected not only by the substituents at the *para*-position of the phenyl ring but also by molecular distribution in the solid state. In particular, the emission colors were changed by heating without crystal phase transition. It was proposed that their thermochromic properties were correlated not with isomerization but with the molecular motion at the distorted benzobithiophene moiety.

Introduction

Thermochromic materials are versatile for thermometers, wide-tunable micro laser crystals and warning signals. There are many thermochromic dyes based on both organic and inorganic compounds such as liquid crystals,[1] stable radicals,[2] polymorphic compounds,[3] conjugated polymers,[4] leuco dyes,[5] Cu_4I_4 clusters[6] and inorganic oxides.[7] Proposed mechanisms of these compounds are classified into 1) the changes in the structure by chemical reactions (i.e. neutral and biradical), 2) crystal phase transition (i.e. liquid crystals and polymorphic compounds), 3) switching of the energy back transfer (i.e. europium complexes), and 4) spin cross-over system (i.e. transition metal complexes).

Combination of "element-blocks", which is defined as a minimum functional unit composed of heteroatoms, with conjugated system is one of valid strategies for fabricating advanced functions.[8] From this view point, the aryl-substituted *o*-carborane skeleton is a promising platform to obtain functional solid-state emissive materials.[9] From the first report on aggregation-induced emission (AIE) which can be detected only in the aggregation and condensed state,[10] the series of solid-state emissive materials were discovered.[11] In particular, stimuli-responsive luminescent chromic behaviors were often found in these materials composed of the *o*-carborane "element-blocks".[12] Therefore, a wide variety of luminescent chromism toward mechanical stresses, temperature changes and vapor fuming were demonstrated with the *o*-carborane-containing conjugated materials.[13] In these materials, luminescent chromism was generally caused by conformational or morphology changes in the solid materials. In order to obtain much sensitive materials, our next goal is to realize luminescent chromic behaviors without drastic structural changes as well as phase transition in the solid state.

We have reported synthesis and optical properties of bis(*o*-carborane)-substituted acenes.[12,14] Intense solid-state emission bands from the intramolecular charge transfer (ICT) state[15] in which the central aromatic system and the *o*-carborane unit respectively worked as an electron donor and acceptor through the carbon in *o*-carborane can be observed in the solid state of these compounds. These *o*-carborane units also played a significant role in suppression of aggregation-caused quenching (ACQ) by disturbing intermolecular interaction because of steric hindrances. Except for luminescent properties, unique structural feature was found from the bis(*o*-carborane)-substituted aromatic ring. It should be remarked that the central anthracene moiety was critically distorted because of the bis(*o*-carborane) substitution according to the X-ray single crystal analyses.[12] From this fact, we presumed that electronic properties of the central distorted aromatic ring could be sensitive toward environmental factors, such as temperature and molecular morphology. In the cooling state or crystalline packing, molecular motions would be highly restricted. Thereby, the distorted center can work as an electron donor, and ICT emission is observable, similarly to the commodity system. Meanwhile, under heating condition or in the solution state, vigorous intramolecular motions should be induced around the distorted center. Therefore, solid-state emission can be varied by external stimuli through perturbation of the electronic state at the distorted center. Based on this assumption, we designed the bis(*o*-carborane)-substituted molecule to demonstrate a luminescent chromic material without structural changes and phase transition.

Herein, synthesis and optical properties of bis(*o*-carborane)-substituted benzobithiophenes are reported. To clarify the structure-property relationship with luminescent behaviors, various substituents were introduced into the *para*-position of the

adjacent phenyl ring in the *o*-carborane unit. From optical and structural analyses, it was found that the synthesized compounds had solid-state emission with the ICT characters, and especially, their emission colors were distinctly altered not only by the substituents at the *para*-position of the phenyl ring but also by molecular distribution in the solid state. Furthermore, thermochromic luminescent behaviors were obtained without crystal phase transition as we expected. Electronic structures at the distorted aromatic core created by the bis(*o*-carborane) substitution should be responsible for luminescent chromism.

Results and Discussion

Synthesis of **DCB-OMe** was performed by employing the previous method for the preparation of **DCB-R** (R = H, ^{t}Bu) as shown in Scheme 1.[16] Benzo[1,2-*b*:4,5-*b'*]dithiophene-4,8-dione was added to the THF solution of the lithiated ethnylbenzene derivative **1-OMe**. Following reduction with the quinone form of benzodithiophene by $SnCl_2$ in the HCl *aq*. solution, the diethynyl derivative **2-OMe** was obtained via the coupling reaction. After the decaborane insertion at the ethynyl moiety, **DCB-OMe** was obtained. **DCB-OH** was prepared by deprotection of the methoxy groups with BBr_3 (Scheme 2). All compounds were characterized by ^{1}H, ^{11}B and ^{13}C NMR spectroscopies (Charts S1−S9), elemental analyses and HRMS measurements. The products showed good stability and solubility in common organic solvents such as $CHCl_3$, CH_2Cl_2, tetrahydrofuran (THF) and benzene. Thus, we concluded that the products should have the designed structures and enough stability for performing the series of measurements.

Schemes 1 & 2

The X-ray single crystal analysis was applicable for determination of the structure of **DCB-OH** (Figure 1). The single crystal of **DCB-OH** was collected by recrystallization from benzene. Although the crystal incorporated benzene as a crystal solvent, π–π interaction between benzene and aromatic rings was hardly observed. Therefore, electronic perturbations to **DCB-OH** by benzene should be negligible. Similarly to the crystal structure of **DCB-H** as reported in the previous study,[12] **DCB-OH** possessed the *cis*-type conformation in the crystal packing. In particular, it was found that **DCB-OH** had intermolecular and intramolecular hydrogen bonds. The distance of intermolecular and intramolecular hydrogen bonds were 1.907 and 1.938 Å, respectively. By the assistance with these hydrogen bonds, **DCB-OH** could be facilitated to form the *cis*-conformation and construct the dimeric structure.

Figure 1

From ^{1}H NMR spectroscopy, the conformations of the compounds were evaluated (Figure S1). In the previous report, it was demonstrated that **DCB-H** can form two types of structural isomers as the *cis*- and *trans*-conformations in the solution state although the *cis*-conformation was dominant in the crystal packing, and these structures were readily distinguishable by the signal patterns in the ^{1}H NMR spectra.[16] Based on this fact, next, to speculate the conformations of **DCB-OMe** and **DCB-CN**, variable-temperature ^{1}H NMR spectra in CD_2Cl_2 were measured (Figure S1). It was known that the signal peak at 8.5 ppm attributable to the *cis*-conformation was small even at low temperature. This result suggests that both compounds should form the *trans*-conformations. The energy differences between the *cis*- and *trans*-conformations of **DCB-OMe** were estimated by

the calculation of thermodynamic parameters with the plot (Figure S2). As a result, it was observed that the enthalpy difference between both conformations was 2.76 kJ/mol, and the *trans*-conformation had more stable than the *cis*-one. Moreover, the peaks assigned to *cis*-conformation of **DCB-CN** were too small to prepare the plot. These data indicate that the **DCB-OMe** and **DCB-CN** should form the *trans*-conformation in the crystal state similarly to **DCB-tBu**. It is likely that steric hindrances of the substituents contributed to formation of the *trans*-conformation.

The UV–vis absorption and photoluminescence (PL) spectra of **DCB-R** in THF (1.0×10^{-5} M) were measured (Figure S3, Table 1). All samples showed the identical absorption spectra. The absorption bands in longer wavelength region had the peaks around 400 nm. These data suggest that the substituent group at the *para* position of the phenyl ring should slightly influence on the electronic structure in the ground state. In contrast, emission wavelengths of **DCB-R** were varied by the substituents. In particular, introduction of cyano groups induced red-shifted emission (Figure S3b). Electron-withdrawing ability of the *o*-carborane units can be enhanced by cyano groups via the σ*−π* conjugation on the C−C bonds in the *o*-carborane unit. Thereby, the emission band should be influenced. It was presumed that emission should be originated from the ICT state according to the previous reports on photophysical properties of the aryl-substituted *o*-carborane derivatives.[9] To confirm this mechanism, UV−vis absorption and PL spectra were recorded in various solvents. Corresponding to the results from these previous reports,[9] the peak positions of absorption bands were detected at the similar positions, while bathochromic shifts were induced by increasing solvent polarity in the PL spectra (Figure S4, Table 2). From the Lippert−Mataga plots in which the extent of slopes of the fitting

line represents the degree of the ICT character in the emission, it was shown that **DCB-R** showed the emission bands from the ICT state. Since the *o*-carborane units can work as a strong electron-accepting unit toward the central benzodithiophene unit, formation of the ICT state should proceed in the excited state.

Tables 1 and 2

Solid-state PL spectra of **DCB-R** were recorded at room temperature. Figure 2 shows the PL spectra in the crystalline state, and the results are listed in Table 1. All compounds showed blue-shifted emission compared to those in the THF solutions. It was implied that re-orientation energy could decrease in the aggregation with *o*-carboranes, and stabilization of the ICT state by solvation could be reduced.[17] As a result, blue-shifted emission bands were detected. The first impressive point is the peak positions of emission bands. Compared to the THF solutions, **DCB-tBu**, **DCB-OMe** and **DCB-CN** which had the *trans*-conformation presented emission bands in the shorter wavelength region than **DCB-H** and **DCB-OH**. In the previous report on the crystal packing of **DCB-tBu**, it was found that intramolecular twist was induced at the benzobithiophene moiety.[16] This conformational distortion should disturb electronic conjugation, followed by emission in the shorter wavelength region. Similar intramolecular twists could occur in **DCB-OMe** and **DCB-CN**. Another feature in the luminescent property was the dependency of emission efficiency on the conformation. Because of larger emission efficiencies in the crystalline state than those in the solution, it was clearly indicated that **DCB-R** had crystallization-induced emission enhancement properties. Moreover, in the crystalline state, the emission efficiencies of **DCB-H** and **DCB-OH** were relatively higher than those

of **DCB-tBu**, **DCB-OMe** and **DCB-CN**. Although the *o*-carborane units located at both sides of the benzodithiophene moiety would suppress ACQ, lower emission properties could be caused by the intramolecular twist in the *trans* conformation of **DCB-tBu**, **DCB-OMe** and **DCB-CN**.

Figure 2

Stimuli-responsiveness of solid-state emission properties of **DCB-R** was evaluated by adding various types of external stimuli to the crystalline samples (Figures 3, 4, 5 and S5). Initially, thermochromic luminescent behaviors were investigated (Figure 3). The emission bands showed bathochromic shifts as temperature increased, and consequently luminescent color was gradually changed by heating (Figure S5). As a representative result, **DCB-OMe** showed the emission band around 570 nm at room temperature, and the bathochromic shift by 20 nm was observed by heating at 200 °C. In particular, it should be emphasized that this luminescent chromism proceeded rapidly and repeatedly (Figure 4). The degree of luminescent chromism seemed to be independent of the conformations. Moreover, from DSC measurements, phase transitions were not observed in the detection temperature range from 0 to 220 °C (Figure S6). It is assumed that intramolecular motions might be induced by heating especially at the benzodithiophene moiety in which distortion of the molecular plane and twists between the connections with the *o*-carborane units were induced.[16] Indeed, emission intensities of all compounds decreased as temperature increased (Figure S7). This fact also supports that intramolecular motions should be activated by heating, and luminescent properties were critically influenced. The crystalline sample of **DCB-OH** showed slight luminescent

chromism. It is likely that intermolecular and intramolecular hydrogen bonds suppressed molecular motions even at high temperature.

Figures 3 and 4

The stimuli-responsiveness of the crystalline sample of **DCB-tBu** toward another external stimulus such as fuming with organic volatile compounds (VOCs) was able to be examined owing to the largest value of emission efficiency in the crystalline state. Interestingly, emission color was changed by exposing other solvents such as benzene, $CHCl_3$, THF, furan and 1,4-dioxane (Figure 5a). In contrast, emission bands were insensitive to vapors of *n*-hexane, toluene, CH_2Cl_2, acetone and MeCN. From the ^1H NMR measurements, it was found that the former solvents can be incorporated into the crystal packing (Figure 5b). Furthermore, from the powder X-ray diffraction analyses, different patterns were obtained from that of **DCB-tBu** with these encapsulated solvents (Figure 5c). Hence, it is suggested that vapochromic luminescent behaviors of **DCB-tBu** should be originated from the crystal−crystal phase transition by insertion of fumed VOCs into the crystal packing. Morphology changes could be reflected to luminescent chromism via the alteration of electronic structures of **DCB-tBu**.

Figure 5

The similar tendencies of a peak position and emission efficiency were also observed by the formation of amorphous states (Table 1). Aggregation was induced by the 100-folds dilution of the THF solution containing 1.0×10^{-3} M **DCB-R** with deionized water.

In the aggregation state, all compounds also demonstrated blue-shifted emission with larger emission efficiency compared to those in the THF solutions. These data mean that **DCB-R** should have the aggregation-induced emission enhancement (AIEE) property. Similarly to the crystalline samples, the molecules having the *trans*-conformation provided emission bands in the shorter wavelength region with larger emission efficiency. Intramolecular distortion could be responsible for optical properties. Significant AIEE was observed from **DCB-OH**. It is likely that intermolecular interaction could be disturbed by the hydrogen bond formation.

Conclusion

Stimuli-responsiveness in the solid-state emissive properties of **DCB-R** via the unique process is demonstrated. Structural diversity was obtained from the derivatives with various types of substituents. In particular, these molecules showed rapid and reversible thermochromic luminescence in the crystalline state. From the series of analyses, the plausible mechanism was suggested. By heating, molecular motions should be activated in the crystalline packing. Then, the room to form thermally-stable conformations could be generated. As a result, extension of conjugated systems could occur, resulting in the bathochromic shifts of luminescence bands. Owing to small structural changes, rapid and reversible responses can be obtained. This strategy to tune luminescent color and to realize thermochromism could be useful for construction the chemical sensors, smart windows, multi-color lasers and molecular thermometers.

ACKNOWLEDGMENT

This work was partially supported by the Asahi Glass Foundation (for K.T.) and a Grant-in-Aid for Scientific Research (B) (JP17H03067) and (A) (JP17H01220), for Scientific Research on Innovative Areas “New Polymeric Materials Based on Element-Blocks (No.2401)” (JP24102013) and for Challenging Research (Pioneering) (JP18H05356).

References

1. I. Sage, *Liq. Cryst.* **2011**, *38*, 1551–1561.

2. a) Y. Morita, S. Suzuki, K. Fukui, S. Nakazawa, H. Kitagawa, H. Kishida, H. Okamoto, A. Naito, A. Sekine, Y. Ohashi, M. Shiro, K. Sasaki, D. Shiomi, K. Sato, T. Takui, K. Nakasuji, *Nat. Mater.* **2008**, *7*, 48–51; b) S. Matsumoto, T. Higashiyama, H. Akutsu, S. Nakatsuji, *Angew. Chem. Int. Ed.* **2011**, *50*, 10879–10883.

3. a) M. C. Torralba, M. Cano, J. A. Campo, J. V. Heras, E. Pinilla, M. R. Torres, *J. Organomet. Chem.* **2001**, *633*, 91–104; b) P. U. Biedermann, J. J. Stezowski, I. Agranat, *Chem. Eur. J.* **2006**, *12*, 3345–3354; c) S. Long, S. Parkin, M. A. Siegler, A. Cammers, T. Li, *Cryst. Growth Des.* **2008**, *8*, 4006–4013; d) P. Naumov, S. C. Lee, N. Ishizawa, Y. G. Jeong, I. H. Chung, S. Fukuzumi, *J. Phys. Chem. A* **2009**, *113*, 11354–11366.

4. a) R. R. Chance, R. H. Baughman, H. Müller, C. J. Eckhardt, *J. Chem. Phys.* **1977**, *67*, 3616–3618; b) R. R. Chance, *Macromolecules* **1980**, *13*, 396–398; c) A. Seeboth, D. Lötzsch, R. Ruhmann, O. Muehling, *Chem. Rev.* **2014**, *114*, 3037–3068.

5. R. Kulčar, M. Friškovec, N. Hauptman, A. Vesel, M. K. Gunde, *Dyes Pigm.* **2010**, *86*, 271–277.

6. a) H. Kitagawa, Y. Ozawa, K. Toriumi, *Chem. Commun.* **2010**, *46*, 6302–6304; b) P. D. Harvey, M. Knorr, *Macromol. Rapid Commun.* **2010**, *31*, 808–826; c) S. Perruchas, C. Tard, X. F. Le Goff, A. Fargues, A. Garcia, S. Kahlal, J.-Y. Saillard, T. Gacoin, J.-P. Boilot, *Inorg. Chem.* **2011**, *50*, 10682–10692.

7. P. Kiri, G. Hyett, B. Russell, *Adv. Mat. Lett.* **2010**, *1*, 86–105.

8. a) Y. Chujo, K. Tanaka, *Bull. Chem. Soc. Jpn* **2015**, *88*, 633−643; b) M. Gon, K. Tanaka, Y. Chujo, *Polym. J.* **2018**, 50, 109−126.

9. a) H. Naito, K. Nishino, Y. Morisaki, K. Tanaka, Y. Chujo, *Angew. Chem. Int. Ed.*

2017, *56*, 254−259; b) K. Nishino, H. Yamamoto, K. Tanaka, Y. Chujo, *Org. Lett*. **2016**, *18*, 4064−4067; c) H. Naito, K. Nishino, Y. Morisaki, K. Tanaka, Y. Chujo, *J. Mater. Chem. C* **2017**, 10047−10054; d) K. Nishino, K. Uemura, K. Tanaka, Y. Chujo, *Molecules* **2017**, *22*, 2009−2018; e) K. Nishino, Y. Morisaki, K. Tanaka, Y. Chujo, *New J. Chem*. **2017**, *15*, 10550−10554; f) H. Naito, K. Uemura, Y. Morisaki, K. Tanaka, Y. Chujo, *Eur. J. Org. Chem*. **2018**, 1885−1890; g) K. Nishino, K. Uemura, K. Tanaka, Y. Chujo, *New J. Chem*. **2018**, *16*, 4210−4214.

10. a) K. Kokado, Y. Chujo, *Macromolecules* **2009**, *42*, 1418−1420; b) K. Tanaka, K. Nishino, S. Ito, H. Yamane, K. Suenaga, K. Hashimoto, Y. Chujo, *Faraday Discuss*. **2017**, *196*, 31−42.

11. a) V. I. Bregadze, *Chem. Rev.* **1992**, *92*, 209−223; b) M. Scholz, E. Hey-Hawkins, *Chem. Rev*. **2011**, *111*, 7035−7062; c) R. Núñez, M. Terrés, A. Ferrer-Ugalde, F. F. d. Biani, F. Teixidor, *Chem. Rev*. **2016**, *116*, 14307−14378; d) F. Issa, M. Kassiou, L. M. Rendina, *Chem. Rev.* **2011**, *111*, 5701−5722; e) R. Núñez, I. Romero, F. Teixidor, C. Viñas, *Chem. Soc. Rev*. **2016**, *45*, 5147−5173; f) R. Furue, T. Nishimoto, I. S. Park, J. Lee, T. Yasuda, *Angew. Chem. Int. Ed*. **2016**, *55*, 7171−7175; g) S. Inagi, K. Hosoi, T. Kubo, N. Shida, T. Fuchigami, *Electrochemistry* **2013**, *81*, 368−370; h) D. Tu, P. Leong, S. Guo, H. Yan, C. Lu, Q. Zhao, *Angew. Chem. Int. Ed*. **2017**, *56*, 11370–11374; i) M. R. Son, Y.-J. Cho, S.-Y. Kim, H.-J. Son, D. W. Cho, S. O. Kang, *Phys. Chem. Chem. Phys*. **2017**, *19*, 24485−24492; j) Y. Chen, J. Guo, X. Wu, D. Jia, F. Tong, *Dyes Pigments* **2018**, *148*, 180−188; k) A. Ferrer-Ugalde, J. Cabrera-González, E. J. Juárez-Pérez, F. Teixidor, E. Pérez-Inestrosa, J. M. Montenegro, R. Sillanpää, M. Haukka, R. Núñez, *Dalton Trans*. **2017**, *46*, 2091−2104; l) Z. Wang, T. Wang, C. Zhang, M. G. Humphrey, *Phys. Chem. Chem. Phys*. **2017**, *19*, 12928−12935; m) X. Li, Y. Yin, H. Yan, C. Lu, *Chem. Asian J*.

2017, *12*, 2207–2210; n) S. Mukherjee, P. Thilagar, *Chem. Commun*. **2016**, *52*, 1070−1093; o) L. Böhling, A. Brockhinke, J. Kahlert, L. Weber, R. A. Harder, D. S. Yufit, J. A. K. Howard, J. A. H. MacBride, M. A. Fox, *Eur. J. Inorg. Chem*. **2016**, 403−412; p) B. H. Choi, J. H. Lee, H. Hwang, K. M. Lee, M. H. Park, *Organometallics* **2016**, *35*, 1771−1777; q) D. Tu, P. Leong, Z. Li, R. Hu, C. Shi, K. Y. Zhang, H. Yan, Q. Zhao, *Chem. Commun*. **2016**, *52*, 12494−12497; r) M. Chaari, Z. Kelemen, J. G. Planas, F. Teixidor, D. Choquesillo-Lazarte, A. B. Salah, C. Viñas, R. Núñez *J. Mater. Chem. C* **2018**, *6*, 11336−11347; s) J. C. Axtell, K. O. Kirlikovali, P. I. Djurovich, D. Jung, V. T. Nguyen, B. Munekiyo, A. T. Royappa, A. M. Spokoyny, *J. Am. Chem. Soc*. **2016**, *138*, 15758−15765; t) K. O. Kirlikovali, J. C. Axtell, K. Anderson, P. I. Djurovich, A. L. Rheingold, A. M. Spokoyny, Organometallics **2018**, *37*, 3122−3131; u) A. M. Prokhorov, T. Hofbeck, R. Czerwieniec, A. F. Suleymanova, D. N. Kozhevnikov, H. Yersin, *J. Am. Chem. Soc*. **2014**, *136*, 9637−9642; v) Y. H. Lee, J. Park, J. Lee, S. U. Lee, M. H. Lee, *J. Am. Chem. Soc*. **2015**, *137*, 8018−8021; w) T. Kim, H. Kim, K. M. Lee, Y. S. Lee, M. H. Lee, *Inorg. Chem*. **2013**, *52*, 160−168; x) N. V. Nghia, J. Oh, J. Jung, M. H. Lee, *Organometallics* **2017**, *36*, 2573−2580.

12. H. Naito, Y. Morisaki, Y. Chujo, *Angew. Chem., Int. Ed*. **2015**, *54*, 5084−5087.

13. a) K. Nishino, K. Hashimoto, K. Tanaka, Y. Morisaki, Y. Chujo, *Sci. China Chem*. **2018**, *61*, 940−946; b) H. Mori, K. Nishino, K. Wada, Y. Morisaki, K. Tanaka, Y. Chujo, *Mater. Chem. Front*. **2018**, *2*, 573–579; c) K. Nishino, H. Yamamoto, K. Tanaka, Y. Chujo, *Asian J. Org. Chem*. **2017**, *6*, 1818−1822.

14. H. Naito, K. Nishino, Y. Morisaki, K. Tanaka, Y. Chujo, *Chem. Asian J*. **2017**, *12*, 2134−2138.

15. a) K. Kokado, Y. Chujo, *J. Org. Chem.* **2011**, *76*, 316−319; b) L. A. Boyd, W.

Clegg, R. C. B. Copley, M. G. Davidson, M. A. Fox, T. G. Hibbert, J. A. K. Howard, A. Mackinnon, R. J. Peace, K. Wade, *Dalton Trans*. **2004**, 2786−2799; c) S. Kwon, K.-R. Wee, Y.-J. Cho, S. O. Kang, *Chem. – Eur. J.* **2014**, *20*, 5953−5960.

16. K. Nishino, K. Uemura, K. Tanaka, Y. Morisaki, Y. Chujo, *Eur. J. Org. Chem*. **2018**, *2018*, 1507−1512.

17. Q. Wu, T. Zhang, Q. Peng, D. Wang, Z. Shuai, *Phys. Chem. Chem. Phys.* **2014**, *16*, 5545–5552.

Figures and Tables

Scheme 1. Synthesis of **DCB-R** (R = H, ^{t}Bu, CN, OMe)

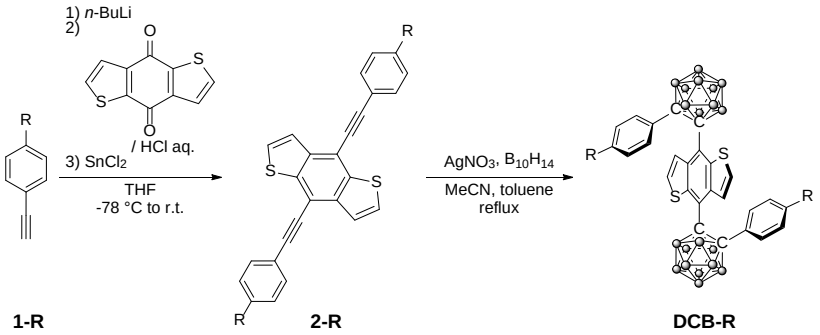

Scheme 2. Synthesis of **DCB-OH**

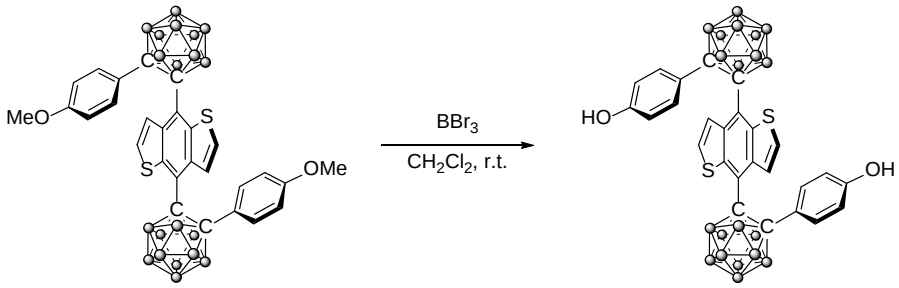

DCB-OMe **DCB-OH**

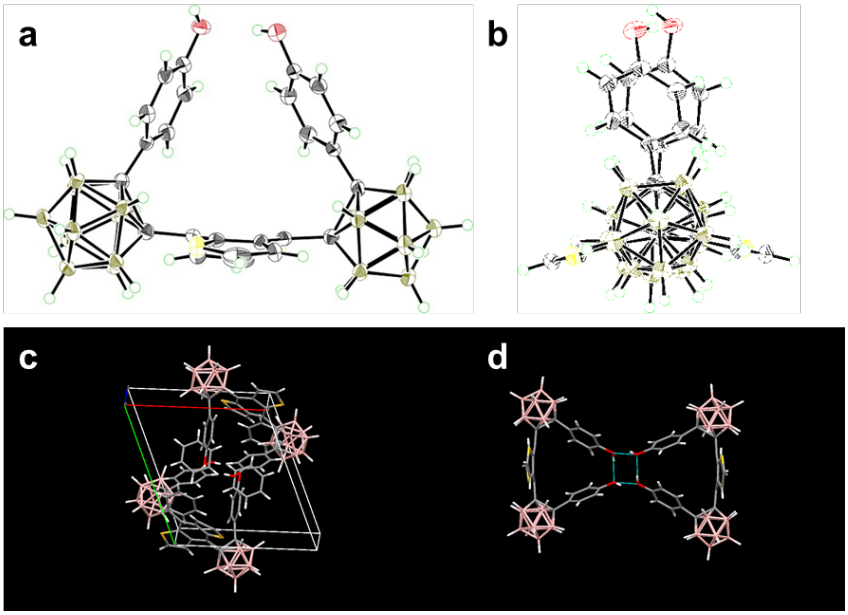

Figure 1. (a, b) ORTEP diagrams, (c) packing structure and (d) hydrogen bonds and dimeric structure of **DCB-OH**.

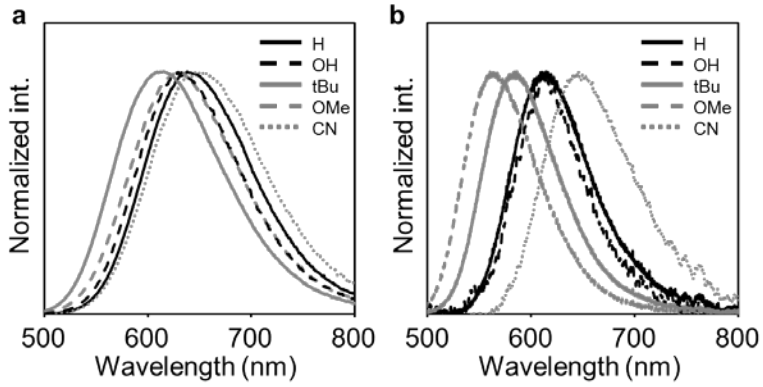

Figure 2. PL spectra in (a) the aggregation and (b) the crystalline state of **DCB-R** at room temperature.

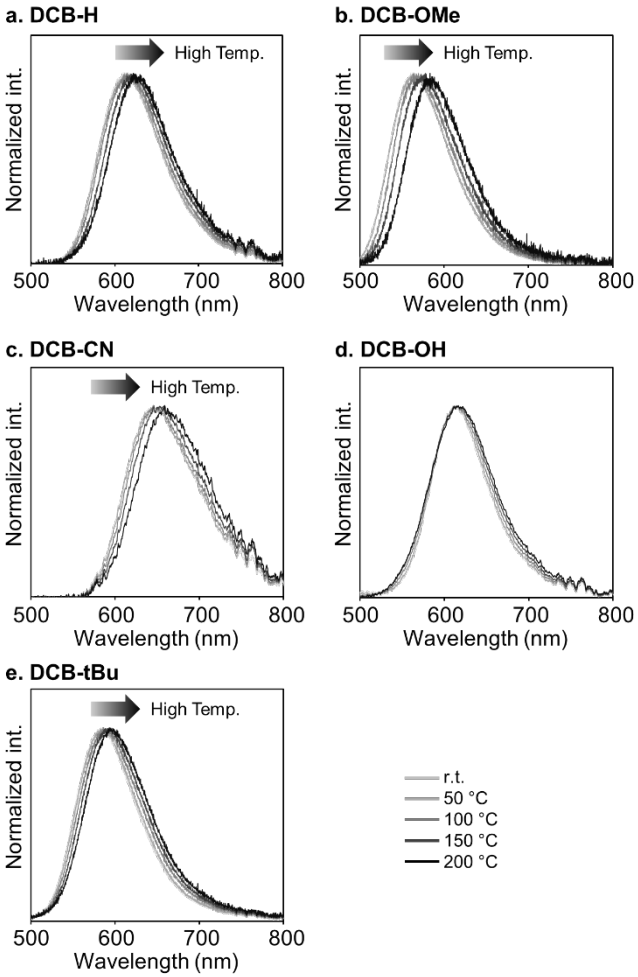

Figure 3. Variable-temperature normalized PL spectra with solid **DCB-R** samples. All samples were placed on the cover glass and heated by a hot plate.

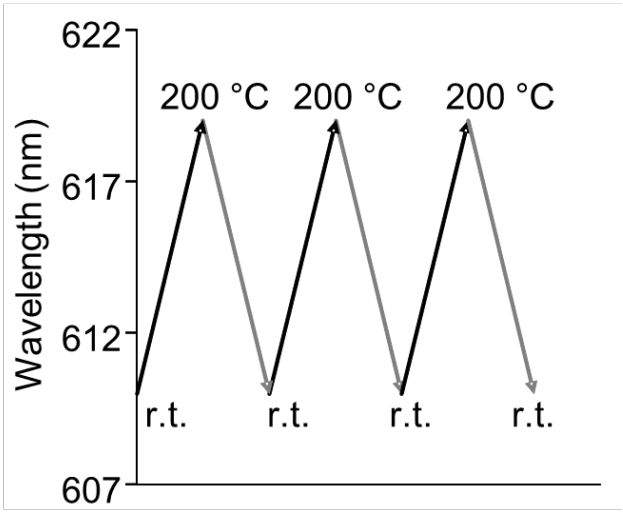

Figure 4. Thermochromism of solid-state emission during stepwise heating and cooling cycles was performed with **DCB-H**.

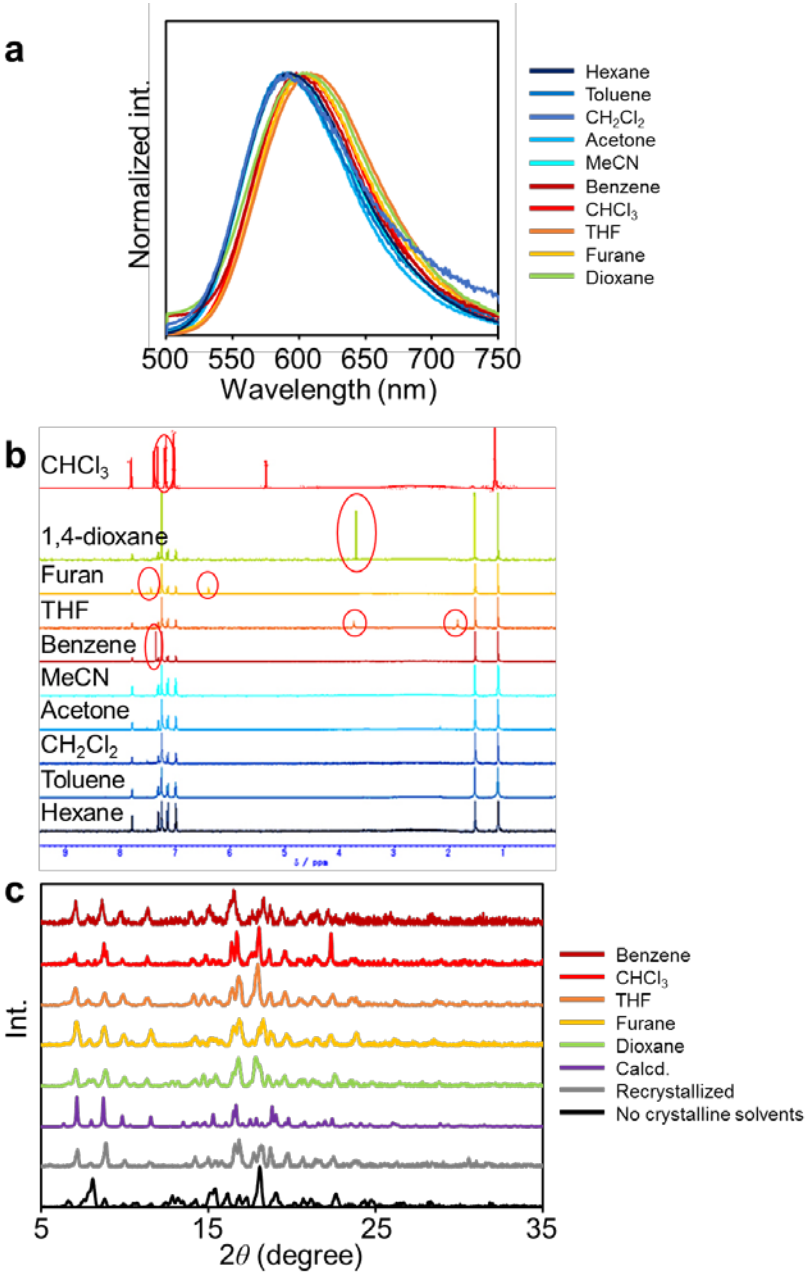

Figure 5. (a) PL spectra (b) ^{1}H NMR spectra in $CDCl_3$ for $CHCl_3$-fumed sample and CD_2Cl_2 for others (red circles: solvent peaks of $CHCl_3$, dioxane, furan, THF and benzene, respectively) and (c) PXRD patterns of **DCB-tBu** after exposing with various solvents.

Table 1. Wavelengths of maximum absorbance and emission and emission efficiencies of **DCB-R** under various conditions

R	λ_{abs}	λ_{THF} (nm)[a]	Φ_{PL}[a,b]	λ_{agg} (nm)	Φ_{PL}[b]	λ_{cry} (nm)	Φ_{PL}[b]
H	403	682	0.12	638	0.23	614	0.90
OH	408	670	0.12	627	0.72	611	0.94
tBu	404	698	0.03	615	0.43	586	0.67
OMe	406	686	0.02	628	0.25	563	0.64
CN	407	727	<0.01	648	0.17	645	0.32

[a] 1.0×10^{-5} M

[b] Determined as an absolute value with the integration sphere method.

Table 2. Summary of changes in optical properties of **DCB-R** by altering solvent types

	DCB-H			**DCB-tBu**			**DCB-OMe**			**DCB-CN**			**DCB-OH**		
solvent	λ_{ab} (nm)	λ_{PL} (nm)	$\Delta\lambda$ (cm^{-1})	λ_{ab} (nm)	λ_{PL} (nm)	$\Delta\lambda$ (cm^{-1})	λ_{ab} (nm)	λ_{PL} (nm)	$\Delta\lambda$ (cm^{-1})	λ_{ab} (nm)	λ_{PL} (nm)	$\Delta\lambda$ (cm^{-1})	λ_{ab} (nm)	λ_{PL} (nm)	$\Delta\lambda$ (cm^{-1})
e	396	603	8668	402	614	8588	400	610	8606	401	624	8912	394	592	8488
benzene	401	658	9740	405	666	9676	406	668	9660	407	682	9907	401	639	9288
$CHCl_3$	400	660	9848	404	670	9827	404	661	9623	405	686	10114	398	635	9377
THF	403	682	10151	404	689	10238	406	686	10053	406	727	10875	402	671	9972
CH_2Cl_2	400	681	10315	405	692	10240	405	685	10092	408	703	10285	398	658	9928
MeCN	402	714	10870	405	722	10840	404	709	10648	405	764	11602	397	686	10611

Graphical Abstract

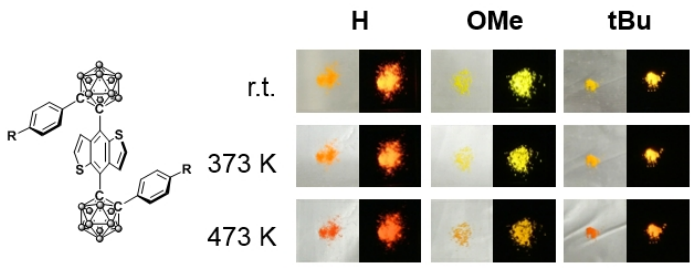

Supporting Information

Design of Thermochromic Luminescent Dyes Based on the Bis(*o*-carborane)-Substituted Benzobithiophene Structure

Kenta Nishino[1], Yasuhiro Morisaki[1,2], Kazuo Tanaka[1]* and Yoshiki Chujo[1]

[1]*Department of Polymer Chemistry, Graduate School of Engineering, Kyoto University, Katsura, Nishikyo-ku, Kyoto 615-8510, Japan*

[2]*Present address: Department of Applied Chemistry for Environment, School of Science and Technology, Kwansei Gakuin University, 2-1 Gakuen, Sanda, Hyogo 669-1337, Japan*

E-mail: tanaka@poly.synchem.kyoto-u.ac.jp

Experimental Section

General. All reagents were obtained from commercial sources and used without further purification. Tetrahydrofuran (THF) was purified using a two-column solid-state purification system (Glass Contour Solvent System, Joerg Meyer, Irvine, CA). ^{1}H, ^{13}C and ^{11}B NMR spectra were recorded on a JEOL JNM-EX400 instrument at 400, 100, and 128 MHz, respectively. Variable temperature ^{1}H NMR spectra were recorded on a JEOL-ECS400 instrument at 400 MHz. The ^{1}H chemical shift values were expressed relative to Me_4Si in $CDCl_3$ or CH_2Cl_2 in CD_2Cl_2 as an internal standard. The ^{13}C shift values were expressed relative to $CHCl_3$ in $CDCl_3$ or CH_2Cl_2 in CD_2Cl_2 as an internal standard. The ^{11}B chemical shift values were expressed relative to $BF_3{\cdot}Et_2O$ as an external standard. High-resolution mass spectra (HRMS) were obtained on a Thermo Fisher Scientific EXACTIVE spectrometer for atmospheric pressure chemical ionization (APCI). Analytical thin-layer chromatography (TLC) was performed with silica gel 60 Merck F254 plates. Column chromatography was performed with Wakogel C-300 silica gel. UV−vis absorption spectra were obtained on a SHIMADZU UV3600 spectrophotometer. Solution state photoluminescence (PL) spectra were obtained on a Horiba FluoroMax-4 luminescence spectrometer; absolute PL quantum efficiencies (Φ_{PL}) were determined using a Horiba FL-3018 Integrating Sphere. Solid state PL spectra were obtained on an Ocean Optics USB 4000. Variable temperature solid-state PL spectra were recorded on a Cimarec™ Digital Stirring Hotplate. X-ray crystal structural analyses were performed with a Rigaku R-AXIS RAPID imaging plate area detector with graphite monochromated Mo *K*α radiation (λ = 0.71069 Å) at −180 ˚C. The structures were solved by direct method (SIR97) and refined by full-matrix least-squares procedures based on F^2 (SHELX-97). X-Ray diffraction (XRD) data were obtained on a Rigaku MiniFlex diffractometer using CuKα radiation in a range of $2° \leq 2\theta \leq 50°$ at intervals of 0.01° at a scanning rate of 0.25° min^{-1}. Differential scanning calorimetry (DSC) thermograms were carried

out on a SII DSC 6220 instrument by using ~10 mg of exactly weighed samples at heating rate of 10 °C/min. Thermogravimetric analysis (TGA) was performed on an EXSTAR TG/DTA 6220, Seiko Instrument, Inc., with the heating rate of 10 °C/min up to 500 °C under nitrogen atmosphere.

Synthesis

General procedure for preparing 4,8-di(arylethnyl)-benzo[1,2-*b*:4,5-*b'*]dithiophenes (2-R).

4-Ethynylaryl (3 eq.) was dissolved in THF under Ar atmosphere. Then, 1.6 M hexane solution of *n*-BuLi (3 eq.) was added to the solution at −78 °C and stirred. After 1 h, benzo[1,2-*b*,4,5-*b'*]dithiophene-4,8-dione (1 eq.) was added in one portion and stirred for 6 h at room temperature. Finally, after adding HCl solution of $SnCl_2$, colored solid was precipitated. The solid was filtered and washed with MeOH, corresponded **2-R** was obtained.

2-OMe: Yellow solid (41%). ^{1}H NMR ($CDCl_3$, 400 MHz) δ = 7.37–7.42 (m, 6H), 7.59 (*d*, 2H, *J* = 5.4 Hz), 7.67–7.70 (m, 4H) 7.71 (d, 2H, *J* = 5.6 Hz) ppm. ^{13}C NMR ($CDCl_3$, 100 MHz) δ = 140.4, 138.3, 131.8, 128.8, 128.5, 123.2, 112.0, 99.2, 85.7 ppm. HRMS (APCI) calcd. For $C_{26}H_{14}S_2$ $[M+H]^+$: 391.0610, found 391.0603.

2-CN: Brownish solid (82%). ^{1}H NMR ($CDCl_3$, 400 MHz) δ = 1.36 (s, 18H), 7.45 (d, 4H, *J* = 8.5 Hz), 7.58 (d, 2H, *J* = 5.6 Hz), 7.62 (d, 4H, *J* = 8.5 Hz), 7.71(d, 2H, *J* = 5.6 Hz) ppm. ^{13}C NMR ($CDCl_3$, 100 MHz) δ = 152.3, 140.3, 138.2, 131.6, 128.0, 125.5, 123.3, 119.9, 112.1, 99.4, 85.1, 34.9, 31.2 ppm. HRMS (APCI) calcd. For $C_{28}H_{12}N_2S_2$ $[M+H]^+$: 441.0515, found 441.0507.

General procedure for preparing 4,8-di(2-arylcarborane-1-yl)-benzo[1,2-*b*:4,5-*b*']dithiophenes (DCB-R).

Decaborane was dissolved in MeCN under Ar atmosphere and heated at 50 °C for 1 h. After the solution turned yellow, toluene was added. Then $AgNO_3$ and **1-R** were added in one portion, and the solution was refluxed over 3 d. The black (or dark red) residue was filtered off and solution was evaporated. The crude residue was purified by silica gel column chromatography. After recrystallization by $CHCl_3$ and MeOH, **2-R** was obtained as colored crystal.

DCB-OMe: Yellow crystal (10%). ^{1}H NMR (CD_2Cl_2, 400 MHz) δ = 7.92 (s, 2H, Ar-*H*), 7.45 (d, 2H, *J* = 5.9, Ar-*H*), 7.17 (dt, 4H, *J* = 2.7, Ar-*H*), 3.62 (s, 6H, C*H*$_3$), 3.43–1.72 (br, 20H, B-H) ppm. ^{13}C NMR (CD_2Cl_2, 100 MHz) δ = 161.8, 144.0, 141.1, 131.6, 126.9, 123.7, 123.6, 123.5, 114.1, 91.6, 88.2, 55.7 ppm. ^{11}B NMR (CD_2Cl_2, 128 MHz) δ =–0.4, –0.6, –2.0, –3.0, –9.3 ppm . HRMS (APCI) calcd. For $C_{28}H_{38}B_{20}O_2S_2$ $[M+H]^+$: 691.4317, found 691.4307.

DCB-CN: Red crystal. (14%). ^{1}H NMR (CD_2Cl_2, 400 MHz) δ = 7.96 (s, 2H, Ar-*H*), 7.50 (d, 2H, *J* = 4.9, Ar-*H*), 7.43 (d, 4H, *J* = 8.8 Hz, Ar-*H*), 7.28(d, 4H, *J* = 8.5 Hz, Ar-*H*), 4.83–1.62(br, 20H) ppm. ^{13}C NMR (CD_2Cl_2, 100 MHz) δ = 143.8, 141.1, 135.7, 132.5, 130.7, 127.7, 123.5, 122.9, 117.6, 115.1, 87.5, 30.3 ppm. ^{11}B NMR (CD_2Cl_2, 128 MHz) δ = –0.4, –0.6, –2.0, –3.0, –9.3 ppm. HRMS (APCI) calcd. For $C_{28}H_{32}B_{20}N_2S_2$ $[M]^-$: 680.3943, found 680.3953.

DCB-OH

DCB-OMe (0.345 mg, 0.5 mol) was dissolved in CH_2Cl_2 (5.0 mL) under Ar atmosphere, and then the solution of BBr_3 in CH_2Cl_2 (1.0 M, 1.05 mL, 1.05 mmol) was added at room temperature. After stirring for 1 h, the reaction was quenched by water, and the organic phase was collected by

a separation funnel. The organic layer was washed with water and brine and dried over $MgSO_4$. After filtration, volatiles were removed by a rotary evaporator. The crude residue was purified by silica gel column chromatography with EtOAc/Hexane (=1/1) as an eluent. After recrystallization from $CHCl_3$ and MeOH, **DCB-OH** was obtained as a red crystal. When an orange crystal was obtained, encapsulation of $CHCl_3$ was observed as a crystal solvent. To remove $CHCl_3$ completely, the crystals were heated at 150 °C for 1 h, and the pure product was obtained as a yellow crystal (0.033 mg, 14%). ^{1}H NMR (CD_2Cl_2, 400 MHz) δ (ppm) 8.49 (s, 2H), 7.65 (s, 2H), 7.08 (d, 4H, J = 8.5 Hz), 6.35(d, 4H, J = 8.6 Hz), 5.2–1.5 (br, 22H). ^{13}C NMR (CD_2Cl_2, 100 MHz) δ (ppm) 157.2, 144.6, 141.2, 132.3, 132.0, 127.8, 124.8, 124.5, 115.9, 94.7, 91.7. ^{11}B NMR (CD_2Cl_2, 128 MHz) δ (ppm) –0.8, –0.2, –3.5, –4.6, –8.6, –9.7. HRMS (APCI) calcd. For $C_{26}H_{34}B_{20}O_2S_2$ [M–H]$^+$: 661.3858, found 661.3839.

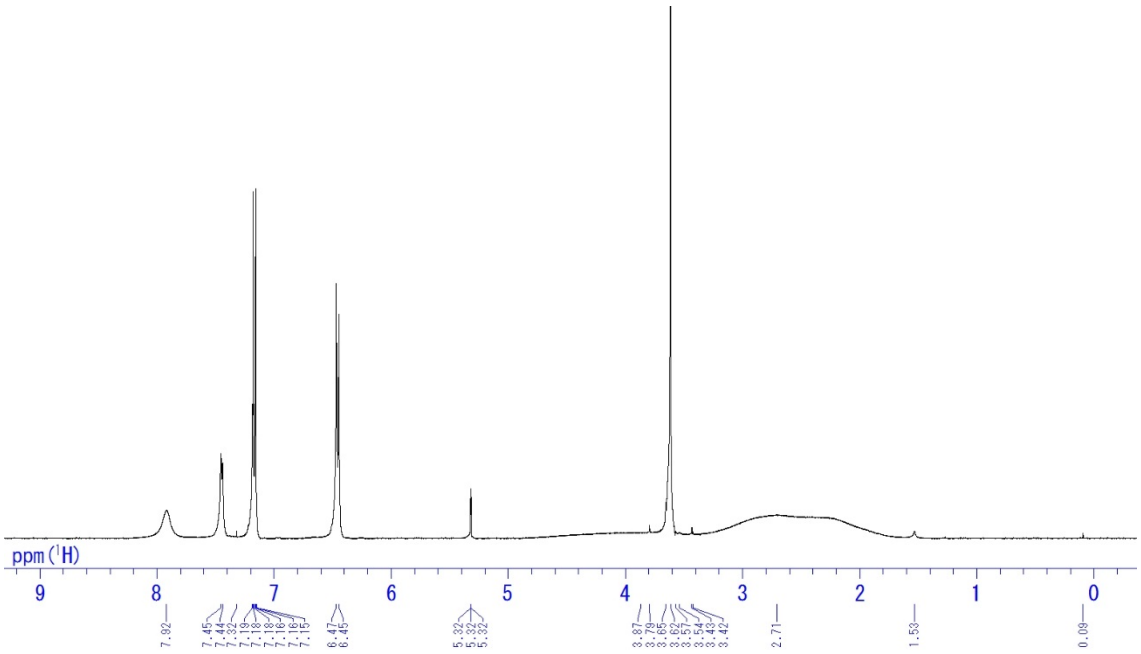

Chart S1. ^{1}H NMR spectrum of **DCB-OMe** in CD_2Cl_2.

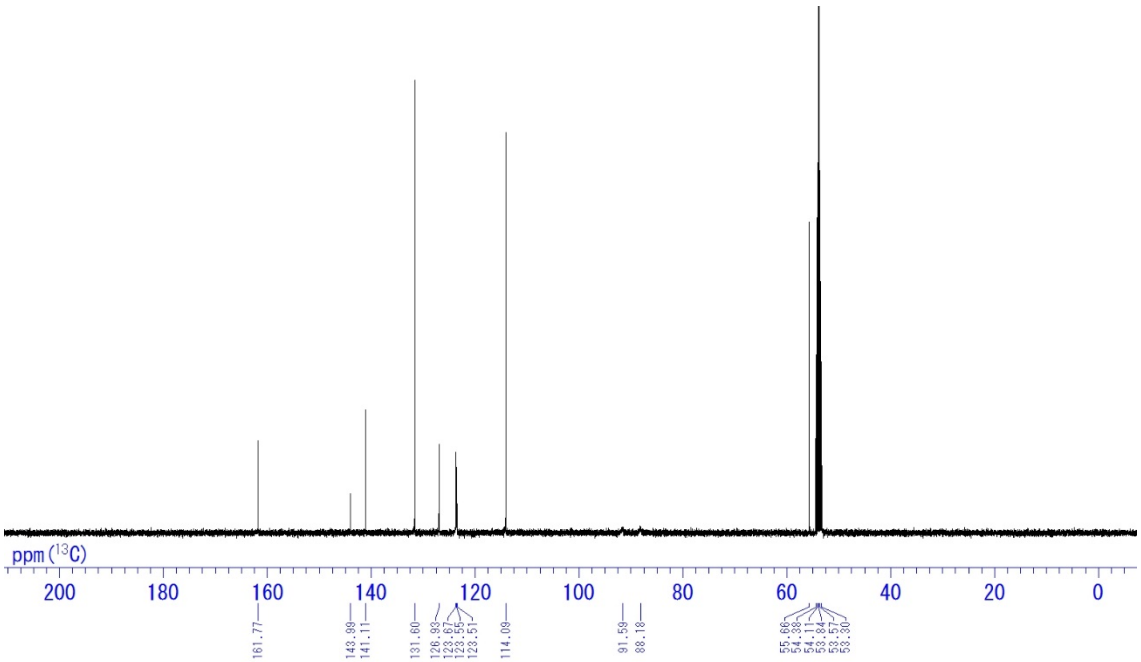

Chart S2. ^{13}C NMR spectrum of **DCB-OMe** in CD_2Cl_2.

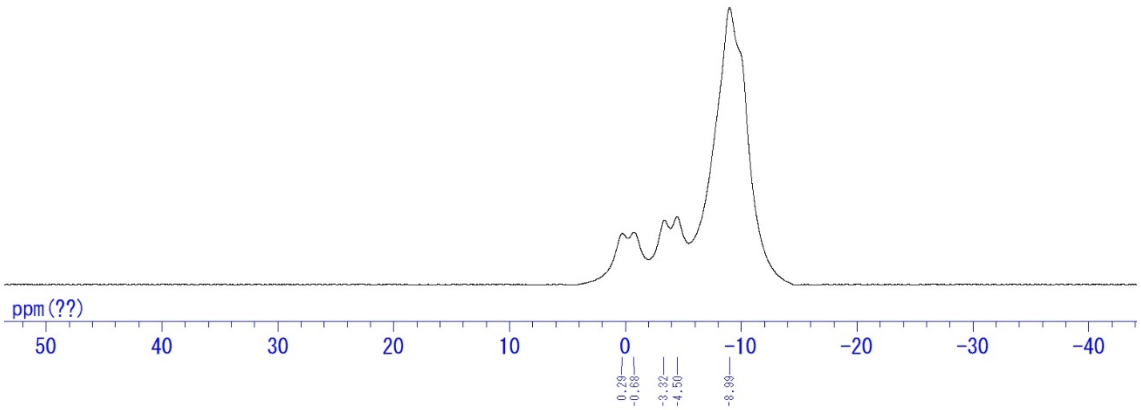

Chart S3. ^{11}B NMR spectrum of **DCB-OMe** in CD_2Cl_2.

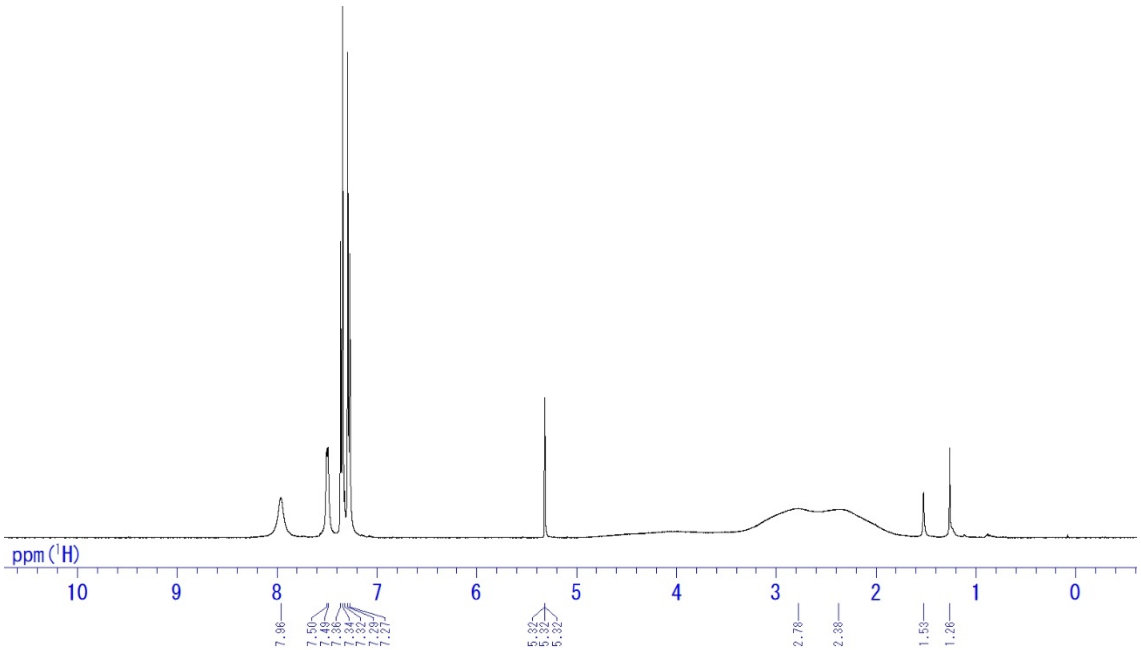

Chart S4. ^{1}H NMR spectrum of **DCB-CN** in CD_2Cl_2.

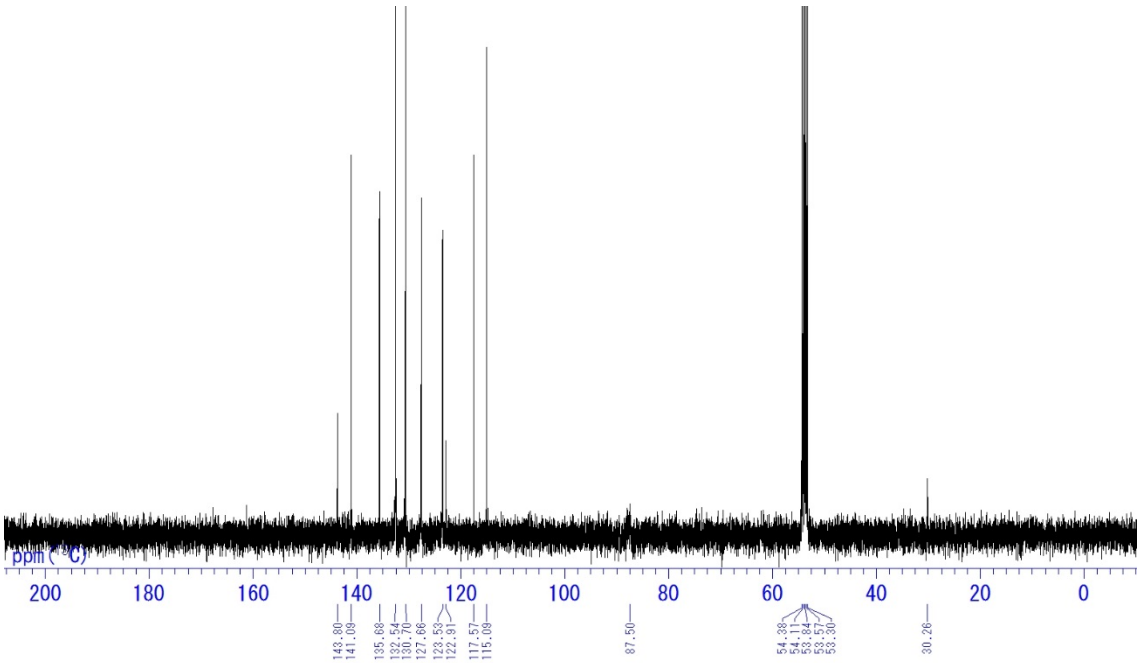

Chart S5. ^{13}C NMR spectrum of **DCB-CN** in CD_2Cl_2.

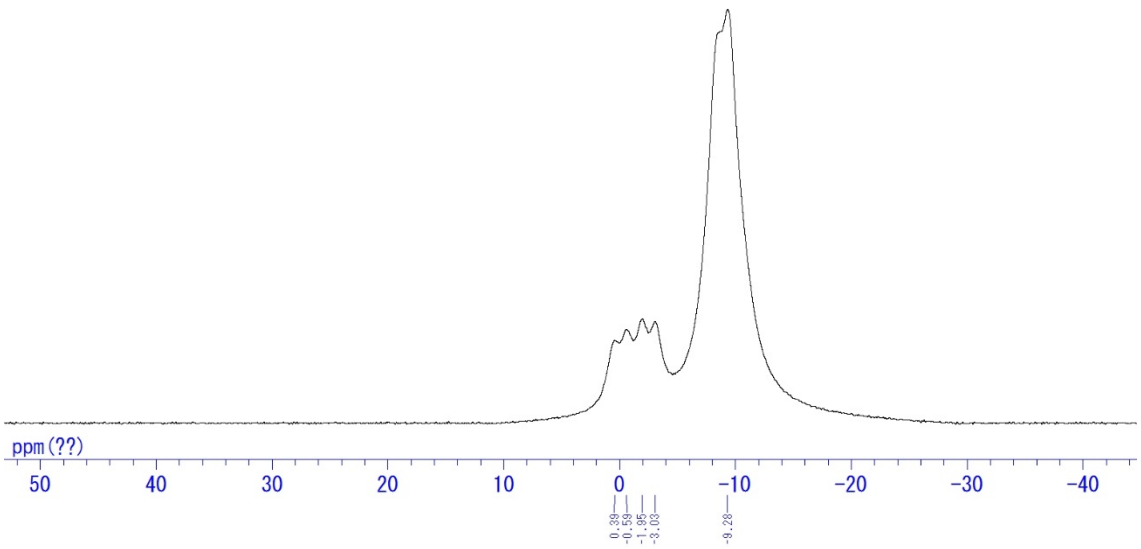

Chart S6. ^{11}B NMR spectrum of **DCB-CN** in CD_2Cl_2.

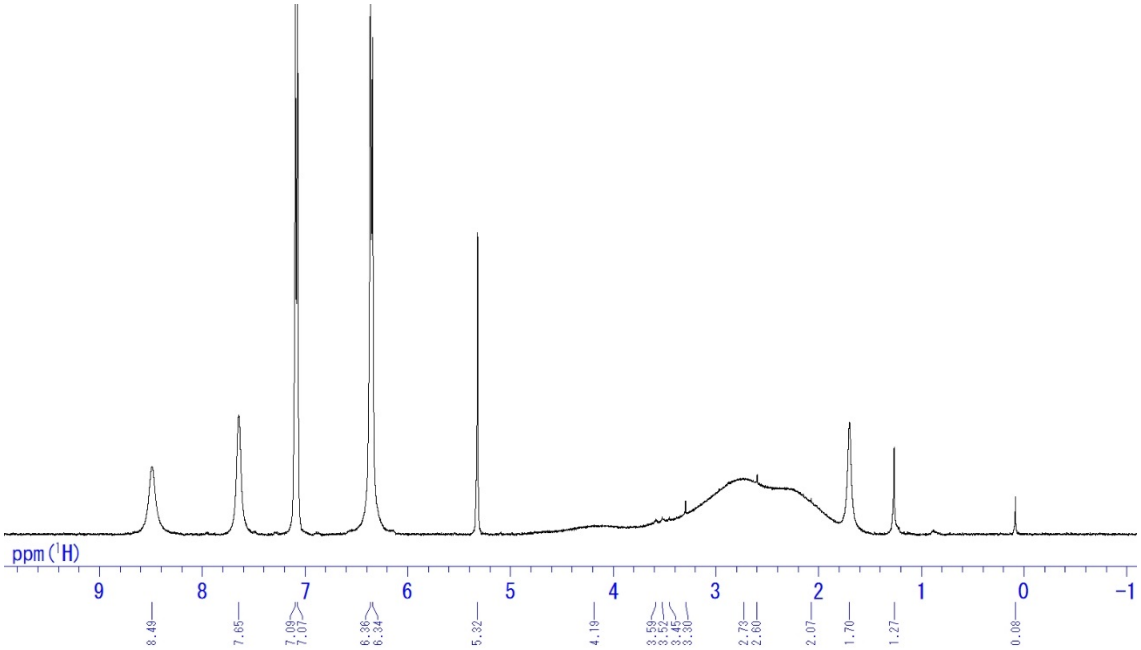

Chart S7. ^{1}H NMR spectrum of **DCB-OH** in CD_2Cl_2.

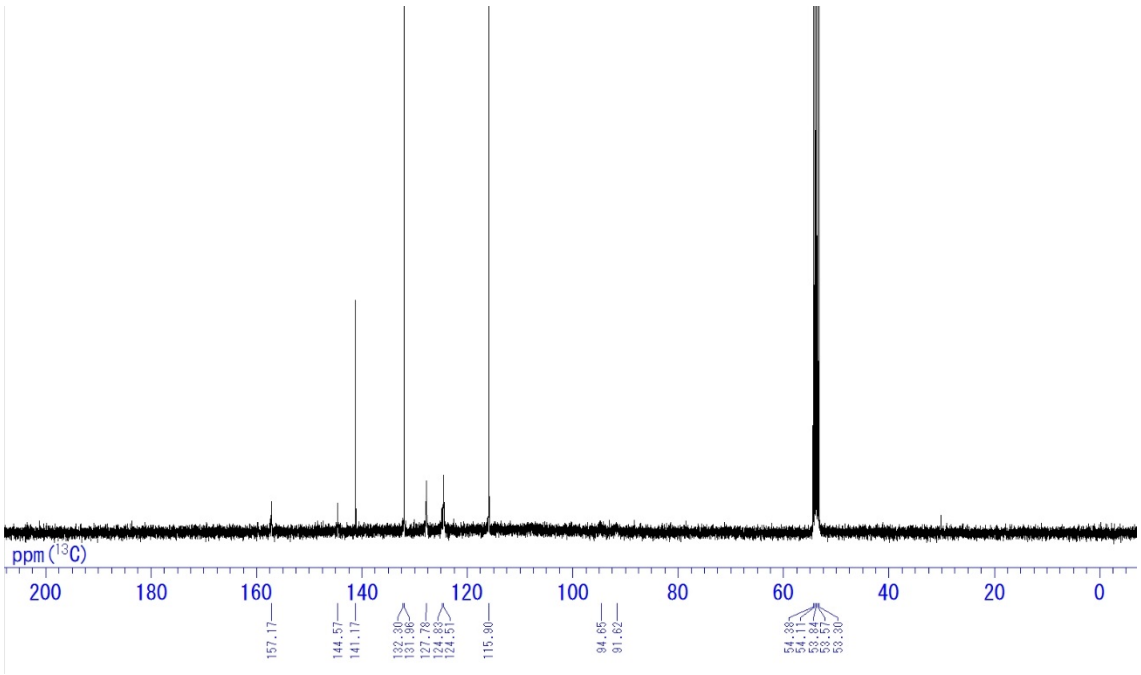

Chart S8. ^{13}C NMR spectrum of **DCB-OH** in CD_2Cl_2.

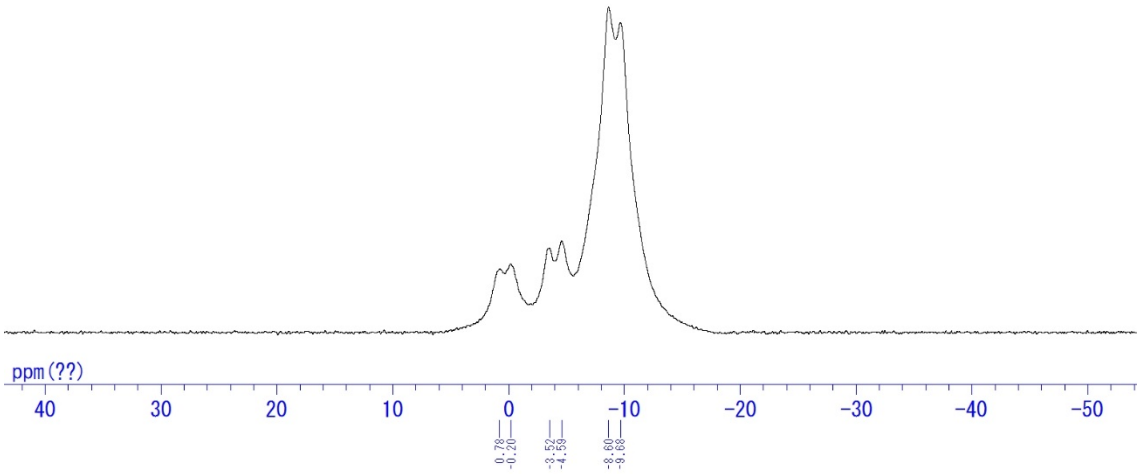

Chart S9. ^{11}B NMR spectrum of **DCB-OH** in CD_2Cl_2.

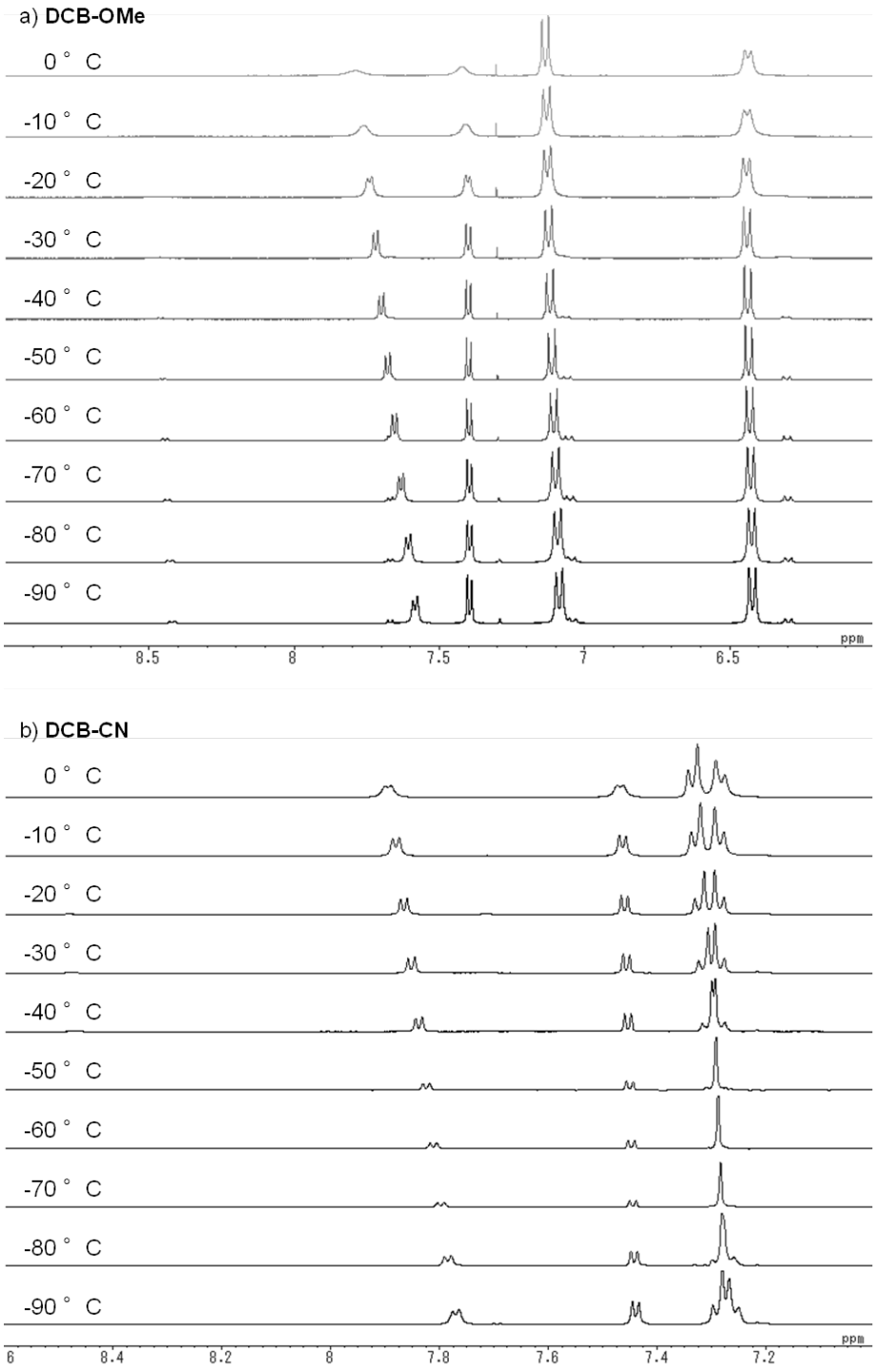

Figure S1. Variable-temperature ^{1}H NMR spectra of a) **DCB-OMe** and b) **DCB-CN** in CD_2Cl_2.

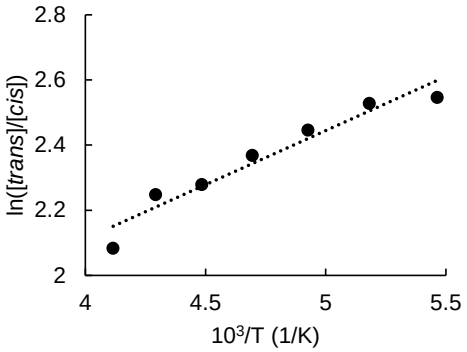

Figure S2. Plots of the *cis-trans* isomerization ratios toward temperature in **DCB-OMe**.

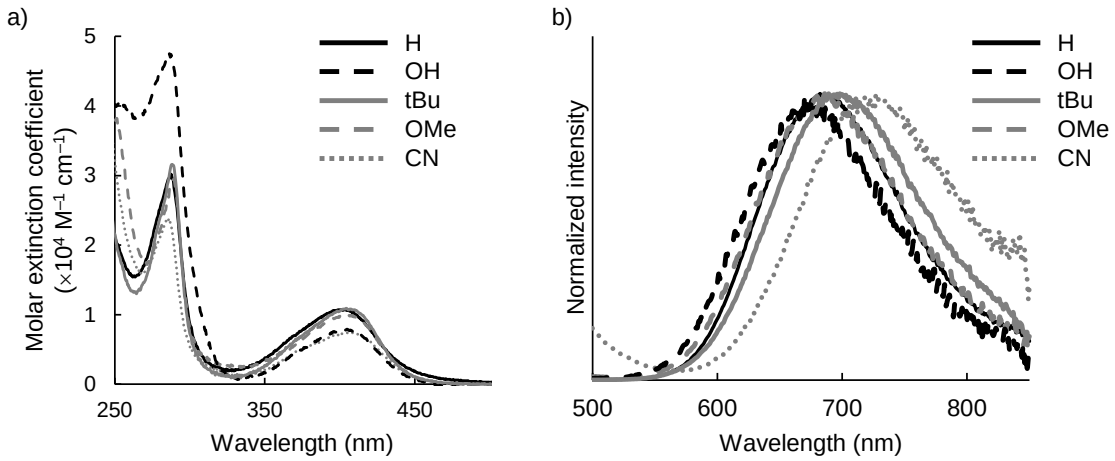

Figure S3. a) UV–vis absorption and b) PL spectra of **DCB-R** in THF.

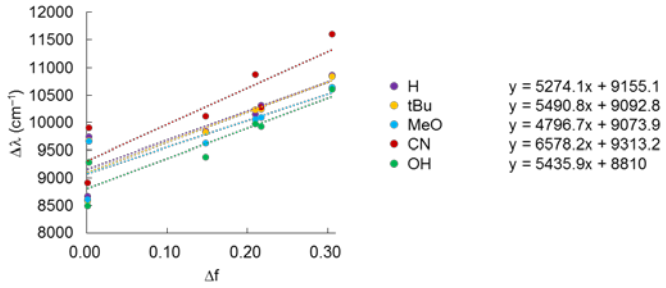

Figure S4. Lippert-Mataga plots with **DCB-R**.

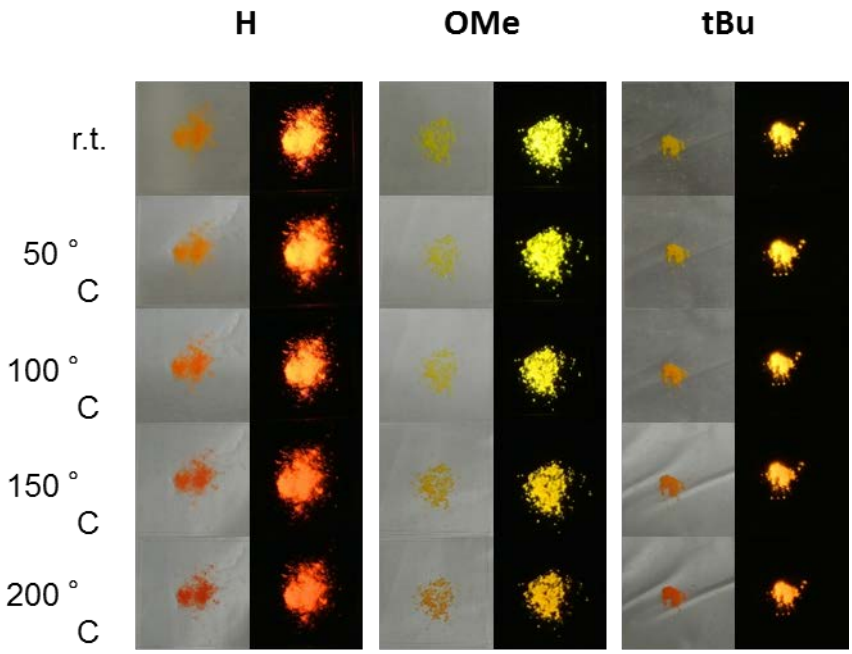

Figure S5. Thermochromic behaviors of **DCB-R**.

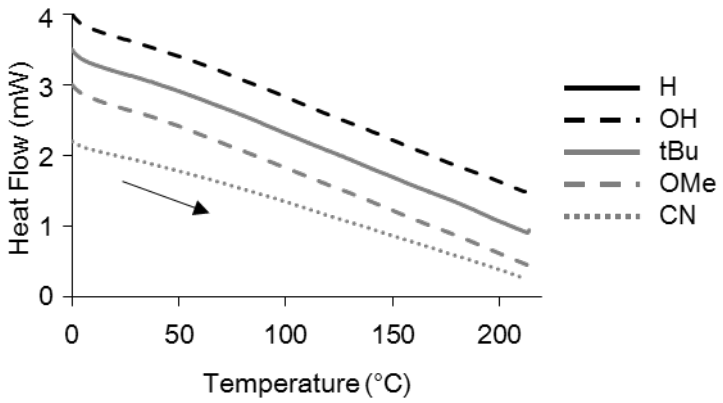

Figure S6. DSC profiles of **DCB-R** with a heating rate of 10 °C/min under N_2 atmosphere.

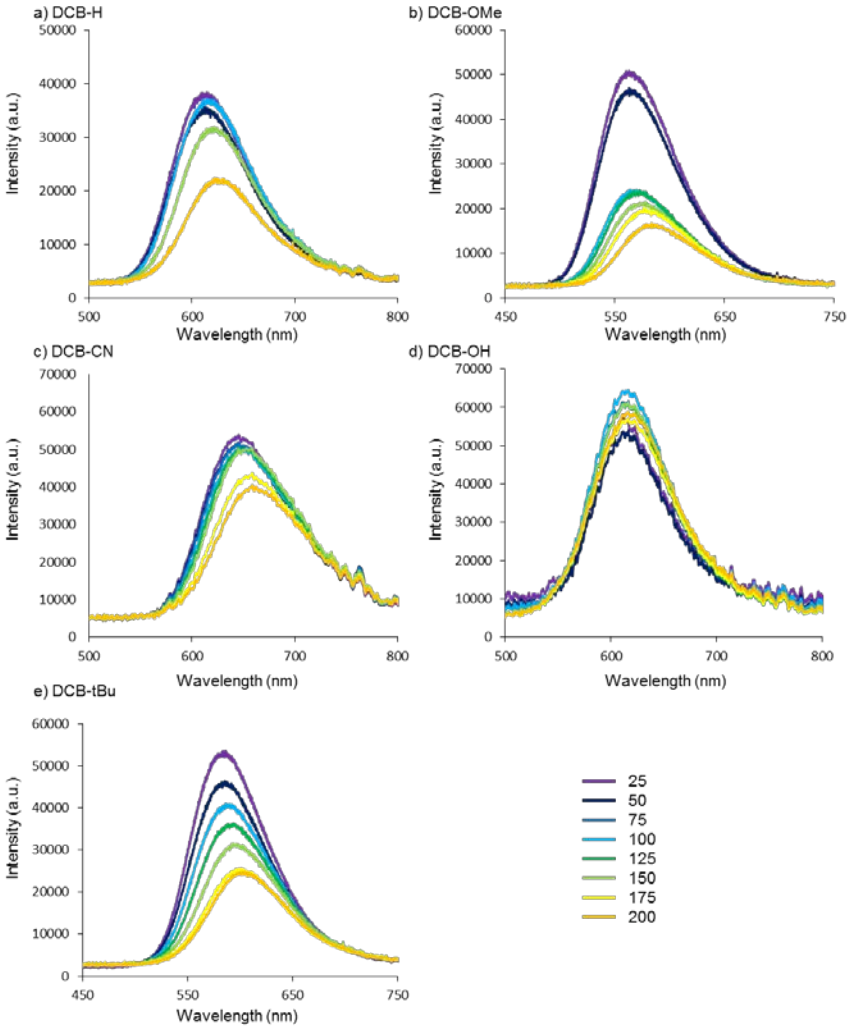

Figure S7. Variable-temperature PL spectra with solid **DCB-R** samples. All samples were placed on the cover glass and heated by a hot plate.

Table S1. Crystallographic data of **DCB-OH**.[a]

Empirical formula	$C_{38}H_{46}B_{20}O_2S_2$
Formula weight	815.07
Temperature (K)	93(2)
Wavelength (Å)	0.71075
Crystal system, space group	Triclinic, *P -1*
Unit cell dimensions	a = 12.712(4)
	b = 12.771(5)
	c = 15.248(5)
	α = 85.190(10)
	β = 70.607(8)
	γ = 66.311(10)
V (Å^3)	2134.7(13)
Z, calculated density (Mg m^{-3})	2, 1.268
Absorption coefficient	0.162
F(000)	844
Crystal size (mm)	0.30 × 0.20 × 0.10
θ range for data collection	3.01 –27.48
Limiting indices	$-16\leq h\leq 16$, $-16\leq k\leq 16$, $-19\leq l\leq 16$
Reflections collected (unique)	20151/9650 [R(int) = 0.1177]
Completeness to theta = 27.482	0.985
Max. and min. transmission	0.953 and 0.984
Goodness-of-fit on F^2	1.022
Final R indices [$I > 2\sigma(I)$][b]	R_1 = 0.0887, wR_2 = 0.1947
R indices (all data)	R1 = 0.1683, wR2 = 0.2420

[a] The structures were solved by direct method (SHELXT)[1] and refined by full-matrix least-squares procedures based on F^2 (SHELX-2014/7).[2] [b] $R_1 = \Sigma(|F_0|-|F_c|)/\Sigma|F_0|$. w$R_2 = [\Sigma w(F^2_0-F^2_c)^2/\Sigma w(F^2_0)^2]^{1/2}$. $w = 1/[\sigma^2(F^2_0)+[(ap)^2+bp]]$, where $p = [\max(F^2_0,0)+2F^2_c]/3$.

[1] G.M. Sheldrick, A short history of SHELX, Acta Cryst. (2008). A64, 112–122.
[2] Sheldrick, G. M. SHELXTL Version 2014/7. http://shelx.uni-ac.gwdg.de/SHELX/index.php.